J Mater Sci (2018) 53:7072–7082

Polymers

A thermally stable and hydrophobic composite aerogel made from cellulose nanofibril aerogel impregnated with silica particles

Jingjing Fu[1], Chunxia He[2], Siqun Wang[3,*], and Yongsheng Chen[1,*]

[1] Nanjing Research Institute for Agricultural Mechanization, Ministry of Agriculture, Nanjing 210014, China
[2] College of Engineering, Nanjing Agricultural University, Nanjing 210031, China
[3] Center for Renewable Carbon, University of Tennessee, Knoxville, TN 37996, USA

Received: 30 August 2017
Accepted: 12 January 2018
Published online: 24 January 2018

ABSTRACT

A thermally stable and hydrophobic cellulose nanofibril (CNF)–silica composite aerogel was prepared by simply immersing the CNF aerogel into the silica sol with different tetraethyl orthosilicate (TEOS) concentration and shaping it by means of low-risk ambient pressure drying. After the introduction of the mesoporous silica particles into the cellulose network structure, the BET surface area was found to have sharply increased from 11.3 to 497.8 $m^2 g^{-1}$. All composite aerogels displayed good thermal stability and super-hydrophobicity compared with pure cellulose aerogel. The onset temperature of pyrolysis rose from 317 to 348 °C, and the contact angle reached 152.1°. The TEOS concentration was found to have a great influence on the silica content and the dispersion of silica particles in the cellulose scaffold. Good chemical compatibility at the nanoscale level was present, which indicates that a continuous and homogeneous CNF–silica interface would yield great improvement in thermal properties and water resistance. The results show that a composite aerogel prepared at 2.5 mol L^{-1} TEOS concentration has better comprehensive performance with only a slightly decrease in mechanical properties compared to CNF aerogel. Thus, this study details a new direction for the synthesis of a cellulose–silica composite aerogel with tailored properties achieved by controlling the silica content and silica dispersion in the cellulose scaffold. Thermally stable, water-resistant, and environmentally friendly cellulose–silica composite aerogels may provide a promising development for designing new functional aerogels that can be applied in various fields.

Address correspondence to E-mail: swang@utk.edu; cys003@sina.com

https://doi.org/10.1007/s10853-018-2034-9

Introduction

Cellulose aerogels constitute a new generation of aerogels that combine the important properties of conventional silica aerogels with their own excellent biocompatibility and biodegradability [1]. The preparation process for cellulose aerogels is carried out in the following three stages. The preliminary process requires lengthy, multiple steps to dissolve the cellulose. This is followed by precipitation in a suitable liquid medium that acts to penetrate the structure and displace the solvent. Induced gelation and solvent exchange follow. The final step involves freeze-drying, supercritical drying [2], and ambient pressure drying [3]. Nowadays, those highly porous, lightweight aerogels could be prepared through benign means and are getting to a stage of commercialization [4].

The development degree of these biomass-based aerogels has already exceeded traditional inorganic aerogels, and an expanding market now exists for different applications, such as absorbents [5, 6], drug release [7], tissue engineering [8], thermal insulation [9], acoustic insulation [10], super-capacitors [11], gas filters [12], sensing materials [13], catalysts [14], and other fields. However, applications for cellulose aerogels have been limited by cellulose's thermolability and hygroscopicity. In order to improve the properties of cellulose aerogels and exploit their many advantages, recent studies have explored surface modification of CNFs by physical, physicochemical, or chemical methods including: plasma deposition [15], chemical vapor deposition (CVD) [16], atomic layer deposition (ALD) [17], alkyl ketene dimer (AKD) modification [18], nanoparticle deposition [19], spin coating [20], and the sol–gel process [21]. Nevertheless, although the above-mentioned methods could facilitate potential functional applications for cellulose aerogels, some defects in the preparation process exist, such as the high cost of synthesis, complicated preparation techniques, the toxicity of ingredients, and only suitability for producing pilot scale products, all of which have dramatically hampered the development and industrial application of cellulose aerogels. Thus, the introduction of easy-to-produce, low-cost, environmentally friendly modifications to cellulose aerogels to get products with value greater than their input value represents a great potential development for cellulose-based aerogels on the commercial market.

Our group recently reported an extraction of cellulose nanocrystal from switchgrass using a sulfuric acid hydrolysis method [22] and preparation of cellulose aerogel through a freeze-drying method [23]. An aqueous nanofibrillated cellulose suspension with homogeneously dispersed cross-linker was freeze-dried to yield a highly porous three-dimensional network. The cellulose aerogel obtained could keep its shape unchanged in water.

The objective of this study is to improve the thermolability and hydrophilicity of cellulose aerogels. We report a simple modification of cellulose aerogel, based on our previous work [24], made by using cellulose nanofibrils with silica particles to fabricate a composite aerogel with good thermostability and hydrophobicity. The interpenetrating structure of the CNF–silica composite aerogel is obtained by simply immersing the CNF aerogel into the silica sol in situ in a two-step sol–gel process [first impregnating with tetraethyl orthosilicate (TEOS)-based solution and then condensing with a base catalyst]. After gelation, aging, and trimethylchlorosilane (TMCS) surface modification of the wet gel, the resulting composite gel is dried using a safe, low-risk method: ambient pressure drying (APD). The effect of the silica content (different silica content was obtained by varied TEOS concentration) on the thermal performance, physical–mechanical properties, and microstructure of the silica-modified CNF aerogel is examined and reported. It is expected that the simplicity of preparation and improved performance of the CNF–silica composite aerogel will broaden its potential application and facilitate large-scale production.

Materials and methods

Materials

Tetraethyl orthosilicate (TEOS, 98% purity), hydrochloric acid (HCl, 12.1 M), ammonium hydroxide (NH_4OH, 1.0 M), ethanol (anhydrous, histological), *n*-hexane ($\geq$ 95%, environmental grade), and trimethylchlorosilane (TMCS, 98%) were purchased from Fisher Scientific and used as received. Cellulose nanofibrils (CNF, solids 2.95%) were purchased from The University of Maine Process Development Center. Cross-linker Kymene™ resin (Ashland Hercules Inc., USA) was purchased

and added into the nanofibril cellulose suspension. Distilled water was used for all preparations.

Preparation of CNF aerogel

Cellulose nanofibril (CNF) aerogels were prepared according to a procedure previously used by our group [23]. The CNFs were centrifuged to 5% solid concentration and mixed with cross-linker resin (5 wt% of solid CNF). The CNF aqueous suspension was poured into a plastic mold containing several grids, each of which measured 58.0 mm in length, 42.6 mm in width, and 43.7 mm in height. The mold was then placed into liquid nitrogen for 4-min rapid freezing, followed by freeze-drying in a vacuum lyophilizer (Labconco Inc., Kansas City, MO, USA) at a temperature of − 51 °C for 3 days. Samples were oven-heated at 120 °C for 3 h to promote cross-linking in order to form a three-dimensional network.

Preparation of CNF–silica composite aerogels

CNF–silica composite aerogels were synthesized in situ in a two-step catalytic sol–gel process. Tetraethyl orthosilicate (TEOS) was used as the silica precursor, HCl as the acid catalyst, and NH_4OH as the base catalyst. In the first step, a solution was prepared by mixing TEOS, ethanol, water, and HCl. In order to prepare composite aerogels with tailored silica content (20–70 wt%), the different concentrations of TEOS (1.5, 2, 2.5, 3, and 3.5 mol L^{-1}) were chosen and obtained by varied molar numbers of the ethanol (Table 1, $x = 7.56$, 4.7, 3, 1.84, and 1.02, respectively). After 90-min stirring of the first-step solution at 60 °C to process the hydrolysis of TEOS, the CNF aerogels were immersed in the first-step solution for 10 min. During the first immersion period, the second-step solution was prepared. The molar ratio of ethanol and water was 5:2.6, and the base catalyst, NH_4OH, was added to adjust the pH value of the solution to 10. The two-step molar ratios are listed in Table 1. When the first immersion of CNF aerogels was finished, the wet aerogels were taken out from the silica source solution, and a second immersion in the second-step solution was performed to process silica condensation. The second immersion time was the same as the first. After the immersion was completed, the samples were taken out and transferred to another container for gelation (2–3 h). The gels were then immersed in ethanol for further gelation and aging. This step was performed at 50 °C for 24 h. During the gelation of the wet gel, further condensation reactions occurred, strengthening the CNF–silica gels. Subsequently, the gels were kept in an ethanol bath at room temperature for 2 days to remove any impurities or water remaining in the pores. The ethanol solution was refreshed every 24 h.

Before the drying process, the wet gels were subjected to a surface modification to avoid structural cracking when drying. To start the modification, the gels underwent solvent exchange with *n*-hexane at 25 °C for 2 days; the *n*-hexane was refreshed every 24 h. The surface modification was performed by immersing the wet gel in TMCS (10%, v/v)/*n*-hexane solution at room temperature for 24 h. Then, the modified wet gel was washed with *n*-hexane to remove the excess TMCS at room temperature for 24 h. Finally, the wet gels were dried at ambient pressure: 5 h at 80 °C. The composite aerogels were labeled as CS*x*-T*y* (*x* represented the expected silica content and *y* represented the TEOS concentration); for example, CS50-T2.5 was the composite aerogel prepared at 2.5 mol L^{-1} TEOS concentration with 50 wt% silica content.

Characterization

The chemical structure of the samples was characterized by Fourier transform infrared spectroscopy (FTIR). The surfaces of the oven-dried (110 °C, 2 h)

Table 1 Molar ratios of participating reactants for two-step sol–gel process

	TEOS	C_2H_5OH	H_2O	HCl	NH_4OH
First step	1	x	1	7×10^{-4}	–
Second step	–	5	2.6	–	Adjust the pH value to 10
Total	1	$x + 5$	3.6	7×10^{-4}	Adjust the pH value to 10

$x = 7.56$, 4.7, 3, 1.84, and 1.02 corresponding to the TEOS concentration of 1.5, 2, 2.5, 3, and 3.5 mol L^{-1}, respectively

composites were scraped and carefully ground to fine powder. Two mg of the samples prepared as described above was dispersed in 200 mg dry potassium bromide (KBr) and further ground to a fine mixture in a mortar. Before FTIR determination, the mixture was preformed by compressing into tablets. FTIR spectra of composite samples were recorded by a Nicolet iS-1063001 FTIR spectrometer (Thermo Fisher Scientific) at the range of 4000 to 500 cm^{-1} and resolutions of 4 cm^{-1} with 16 scans.

The bulk densities were estimated by dividing the individual masses of the samples by their volumes. The porosity of the aerogel was calculated according to the following equation:

$$\text{Porosity}\ (\%) = \left(1 - \frac{\rho}{\omega_s \cdot \rho_s + \omega_c \cdot \rho_c}\right) \times 100\%$$

where ρ, ρ_s, and ρ_c are the bulk density of the composite aerogels, the skeletal density of the pure silica, and the skeletal density of the cellulose, respectively. Herein, ρ_s and ρ_c were designated to be 2.1 and 1.56 g cm^{-3}, respectively [25, 26]. The silica particle content of the composite aerogel was calculated as follows:

$$SiO_2\%(w/w) = \frac{m_1 - m_0}{m_1} \times 100\%$$

where m_0 and m_1 are the weights of CNF aerogel before and after deposition of the silica particles, respectively.

The Brunauer–Emmett–Teller (BET) test was carried out to determine the surface area of samples. This measurement was taken using N_2-adsorption analysis at 77 K (Gemini VII Micromeritics). The Barrett–Joyner–Halenda (BJH) analyses were done from the adsorption isotherm when the pore size distribution was investigated.

Crystal structures were identified by X-ray diffraction techniques (XRD) using X-Pert Powder (PANalytical B. V., Netherland) operating at a scan rate (2θ) of 10° min^{-1} at an accelerating voltage of 40 kV and an applied current of 300 mA ranging from 5° to 40° with 6 scans.

The morphology of the samples was studied with a Zeiss Auriga SEM/FIB crossbeam workstation (Germany). Samples were sputter-coated with gold–palladium and operated at 2–3 kV. The structure of silica particles on the nanocellulose fibers and the particles' dimensions were obtained from the SEM images.

Samples were subjected to thermogravimetric analysis (TG) in a TG analyzer (PerkinElmer 7 series, PerkinElmer Cetus Instruments, USA). The operating conditions were the following: temperature range of 50–800 °C, with a heating rate of 10 °C min^{-1} (under air atmosphere).

The compressive modulus and compressive strength of the samples were measured using an INSTRON 5567 universal testing machine (Canton, MA, USA) with a 50-kg load cell at a strain rate of 0.2 mm min^{-1}.

The contact angles of the samples were determined from the water drop shape when placed on the sample surface (JC2000D1 contact angel meter, POWERACH, Shanghai, China).

Fire performance of aerogels was performed according to GB/T 2406-93 using by a JF-3 Oxygen Index (OI) Chamber (Nanjing Jiangning Analytical Instrument Co., Ltd, Nanjing, China). In the OI test, all samples were placed in a vertical glass column using a sample holder, and adjusted gas flow (oxygen and nitrogen) to confirm the standard test technique. Each sample was ignited with a flame and was burned downward into the unheated material. The minimum oxygen concentration which supported the combustion for all samples was recorded as a percentage.

Results and discussion

Physical properties and morphology

A summary of the physical properties of the pure cellulose aerogel and CNF–silica composite aerogels with different silica content is given in Table 2. There were small differences between the expected and measured value of silica content. But the silica content of composite aerogels did not increase with increasing TEOS concentration; this behavior may be owing to the interaction between the TEOS concentration and the pH value of condensation process. Based on previous study, a higher pH value resulted in higher silica content, and a higher TEOS concentration would result in a faster condensation [27]. Thus, the varied TEOS concentration would certainly affect the condensation of silica particles, which induced the erratical growth of silica particles. The bulk density and porosity of aerogels were controlled by the silica content in the matrix. The CNF aerogel exhibited small BET surface area, ultra-low density, and extremely high porosity (≥ 96%). The addition of

Table 2 Bulk density, silica content, porosity, specific surface area, and pore size distribution of CNF aerogel and CNF-silica composite aerogels

Sample ID	Bulk density (g cm^{-3})	SiO_2 in aerogel (wt%)	Porosity (%)	Specific surface area (m^2 g^{-1})	Pore radius (nm)	Pore volume (cm g^{-1})
CNF	0.055 (0.002)	0	96.46	11.3	8.3	0.0853
CS20-T3	0.067 (0.001)	19.72 (0.36)	95.97	70.31	1.678	0.1991
CS40-T2	0.096 (0.005)	42.71 (2.33)	94.62	203.02	1.893	0.2606
CS50-T2.5	0.117 (0.009)	50.13 (0.92)	93.62	469.70	1.913	0.623
CS60-T1.5	0.140 (0.007)	60.70 (1.30)	92.58	497.84	1.892	1.036
CS70-T3.5	0.160 (0.010)	66.36 (3.36)	91.63	398.73	1.897	0.6524

The data in parentheses are the standard deviation

the silica particles resulted in a further increase in bulk density and a slight decrease in porosity. That more silica particles filled in the cellulose pore structure was accordingly reflected in the decrease in porosity, and the thickness of the fiber skeleton led to the increasing density. In addition, a bump increase in the BET surface area with the increasing mass content of the silica phase and the filling in of nanoscale SiO_2 microspheres into the cellulose web-like pore structure were found to significantly contribute to the overall surface area. However, this tendency was not seen in the sample CS70-T3.5 with 66.36 wt% silica content; there, the surface area of CS70-T3.5 showed a small decrease compared with that of the CS60-T1.5 (60.7 wt% silica content). This difference may be attributed to the degree of distribution of silica particles in the cellulose matrix. From the data of pore size distribution, the CNF aerogel had larger pore radius and smaller pore volume compared with composite aerogels, and those had little difference among composite aerogels. The smaller pore radius the aerogel has, the larger the BET surface area will be. And the BET surface area also depends on the pore volume: larger pore volume will bring larger BET surface area. This great difference between CNF aerogel and composite aerogel was that the secondary silica particle ring occupied and parted off the pore structure of cellulose fibers, which contributed to the increase in pore volume and decrease in pore radius.

The different TEOS concentrations could affect the output of silica particles and their condensation form; the SEM images of the CNF aerogel and the composite aerogels may represent the existence of a form of SiO_2 in the composite aerogels (Fig. 1). The CNF aerogel exhibited a complex porous structure (Fig. 1a); in the sample CS20-T3 (Fig. 1b), due to the coating effect of silica particles, the cellulose fiber grew "thicker," but the size of the individual silica particles varied significantly because of the higher TEOS concentration; in the CS40-T2 aerogel, some of the cellulose fibers were linked together by silica and also formed a few agglomeration in the bottom left corner of Fig. 1c; the composite aerogel CS50-T2.5 showed a homogeneous cellulose cross-linked structure with silica (Fig. 1d), which indicated that the CNF aerogel had become impregnated into the silica sol, enhancing the strength of the connections between the cellulose fibers. In the sample CS60-T1.5 (Fig. 1e), the cellulose fiber was thickened with silica particles and some severe agglomeration of silica particles began to appear, while in CS70-T3.5 (Fig. 1f), most fiber structures were covered by large amounts of silica cluster; this phenomenon could be explained that the silica would experience fast condensation when penetrated into the cellulose structure at this TEOS concentration, forming a layered structure: a layer with larger silica content wrapped around the core layer with relatively less silica content. The SEM image of CS70-T3.5 displaying considerably agglomerated silica particles also could confirm the reason for the decrease in the surface area. In other words, the composite aerogel seems to have exhibited a more unstable structure and heterogeneous silica dispersion when prepared at higher TEOS concentration (≥ 3 mol L^{-1}), which may have weakened the functional properties of the composite aerogel. While in the lower TEOS concentration (≤ 1.5 mol L^{-1}), due to the synergistic effect of TEOS concentration and pH value, the composite aerogel would also exhibit incompatibility microstructure. Therefore, the TEOS concentration of the first-step impregnation atmosphere should not exceed 2.5 mol L^{-1} and not lower than 1.5 mol L^{-1}.

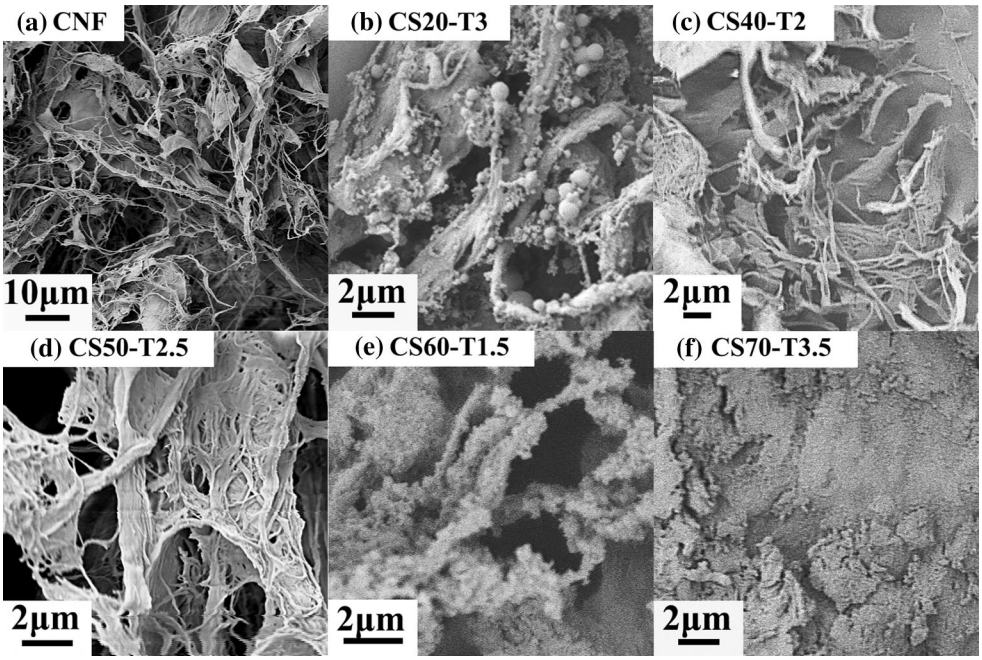

Figure 1 SEM images of **a** CNF aerogel and composite aerogels, **b** CS20-T3, **c** CS40-T2, **d** CS50-T2.5, **e** CS60-T1.5 and **f** CS70-T3.5.

Fourier transform infrared spectroscopy (FTIR) analysis

The silication of the cellulose nanostructure was monitored by FTIR spectroscopy (Fig. 2). As expected, all five CNF–SiO_2 composite aerogels displayed similar spectra and were clearly different from the spectra of CNF aerogel in some ranges. Spectrum measurements over a wide band in the region between 3600 and 3200 cm^{-1} were taken in all samples, which is characteristic from the vibration of the –OH groups present in the cellulose molecules [28, 29]. In the composite aerogels, the intensity of the absorbance band in this region was seen to slightly

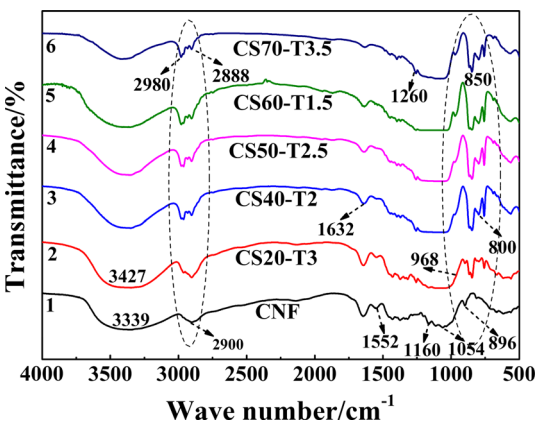

Figure 2 FTIR spectra of CNF aerogel and composite aerogels.

shift to a higher wave number in comparison with that of CNF aerogel (The center shifted from 3339 to 3427 cm^{-1}). This band also represented the combination of characteristics of the cellulose and nano-SiO_2 in that the carboxylic groups of cellulose are capable of forming intermolecular hydrogen-bonding with the silanol groups (asymmetric vibration of Si–OH) on the surface of the inorganic network produced in the sol–gel process. An absorption peak at 1632 cm^{-1} was the O–H bending vibration peak of water with trace impurities absorbed by the cellulose [30]. As compared with the cellulose aerogel, the peak at 1632 cm^{-1} of cellulose–silica composite aerogels was weaker, indicating that the hydrophilicity of the composite aerogels was weaker. A new weak peak arising at 1552 cm^{-1} was attributed to N–H bending of the amide, suggesting that the cross-linker Kymene™ was indeed bonded to the cellulose after heat treatment [31]. In the CNF aerogel, the peak appearing at 2900 cm^{-1} was attributed to aliphatic C–H stretching in methylene groups [32] and that appearing at 1160 cm^{-1} was attributed to the C–O–C asymmetric stretching vibration from the glycosidic ring [33]; the peak at 1054 cm^{-1} was assigned to C–O symmetric stretching of primary alcohol and that at 896 cm^{-1} showed the b-Glucosidic linkages between the glucose units [28]. In comparison with cellulose aerogel, the composite aerogels

were observed to have their own absorption peaks. The peaks at 968 and 800 cm^{-1} represented the asymmetric vibration of Si–OH and Si–O–Si, respectively [34, 35]. Those located at 1260, 850 cm^{-1} were attributed to the attachment of Si–CH_3 onto the silica backbone, and the presence of the trimethylsilyl group manifested the effect of surface modification using TMCS [36]. A wide flat band between 1200 and 1050 cm^{-1} could be assigned to the Si–O–C bond. These absorption peaks perhaps indicate that the –CH_3 groups were incorporated into the Si–O–Si chain structure [37]. The formations of those functional groups mean that the silica particles have intimate interaction with cellulose chains, which indicates a successful preparation of cellulose–silica composite aerogels at the molecular structure level.

X-ray diffraction techniques (XRD) analysis

The XRD patterns and crystallinity of CNF aerogel and CNF–silica composite aerogels are displayed in Fig. 3. The pure cellulose aerogel exhibited a distinct peak at $2\theta = 22.5°$, corresponding to the (002) lattice planes of cellulose I; the overlapping peaks at $2\theta = 14.0°–17.0°$ can be indexed as the (101) and $(10\bar{1})$ lattice planes of the cellulose I crystalline structure [38–40], and the signal at 34.2° can be ascribed to the (040) plane of cellulose I crystal structure [41]. For the XRD patterns of the CNF–silica composite aerogels, the height of the peak observed at 22.5° decreased, but we did not find a significant statistical correlation between the intensity of this peak and the silica content of composite aerogels. Another difference between the pure cellulose aerogel and the composite aerogels was that the composite aerogels did not display any crystalline peaks at $2\theta = 14.0°–17.0°$ and 34.2°. The crystallinity data (C_I, refined and calculated by JADE software) could further reveal the compositional variation of the matrix: with increasing silica content (in other words, the decrease in cellulose content in the matrix), the crystallinity of the composite aerogels decreased gradually. An explanation of this behavior may be that the existence of silica particles had disrupted the bonding of microfibrils into ribbons. It also indicated that the silica in the composite aerogels was amorphous.

Thermal properties

Thermogravimetric analysis (TG) is one of the most important methods for observing the thermal characteristics of materials. TG curves of the CNF aerogels and CNF–silica composite aerogels are presented in Fig. 4, and the TG properties and the silica content of composite aerogels are listed in Table 3. The pure CNF aerogel showed a small weight loss below 120 °C that could correspond to the release of moisture; however, there was no obvious weight loss in other five composite aerogels. It was noted that the cellulose fiber was hydrophilic and that the cellulose aerogel was able to absorb a small amount of water when kept in a sealed condition. The interpenetration of silica particles into the cellulose skeleton apparently lowered the hygroscopicity of the composite aerogels. When the samples were subjected to continuous heating from 50 to 800 °C in air conditions, the CNF aerogel was totally burnt out. In addition, the residual weights of the composite aerogels were consistent with the silica content in the composite aerogels (almost equal), the higher silica content resulting in a larger residual weight. The onset

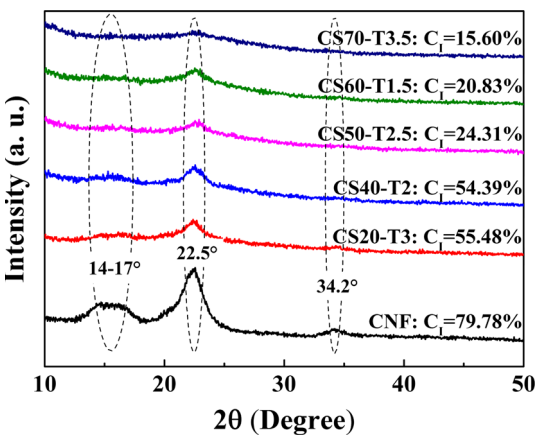

Figure 3 XRD patterns of CNF aerogel and composite aerogels.

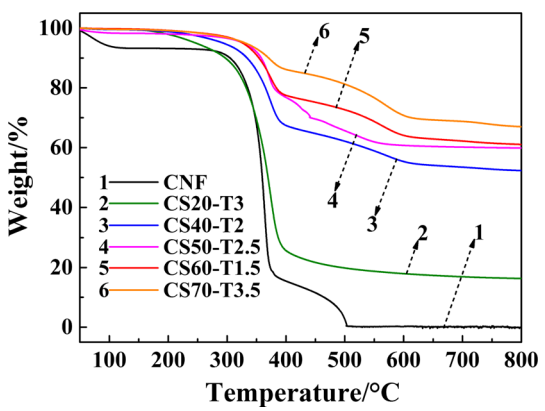

Figure 4 TG curves of CNF aerogel and composite aerogels.

Table 3 TG properties and silica content of CNF aerogel and composite aerogels

Sample ID	Onset temperature (°C)	Residual weight (%)	SiO_2 in aerogel (wt%)
CNF	317.0	0	0
CS20-T3	339.4	16.25	19.72
CS40-T2	334.8	52.24	42.71
CS50-T2.5	348.7	59.83	50.13
CS60-T1.5	336.4	61.02	60.70
CS70-T3.5	328.5	66.86	66.36

temperatures of all composite aerogels were higher than that of the pure cellulose aerogel, indicating that the deposition of silica nanoparticles contributed to improving the thermal stability of the cellulose fibers. Based on the above inferences, the thermal degradation degree should correlate with the silica content; however, in this work there was no positive relationship between the onset degradation temperature and the silica content. The better thermal stability of the aerogel was manifested in composite aerogel prepared with 2.5 mol L^{-1} TEOS concentration, which contained 50.13 wt% silica particles. We reason that the silica particles attached to the nanocellulosic scaffold could promote the thermal stability of the cellulose matrix. However, permitting either a lack of growth or overgrowth of discontinuous and heterogeneous silica particles within the cellulose network skeleton would likely limit the nanoscale compatibility between the organic and the inorganic phases, which would affect the thermal decomposition of composite aerogels.

Based on the TG analysis, the composite aerogel CS50-T2.5 was selected to take comparison with pure CNF aerogel for the combustion test. The oxygen index (OI) is the smallest oxygen concentration, expressed as volumetric concentration, in a mixture of oxygen with nitrogen, introduced at ambient temperature, at which combustion of the materials sample is maintained in specific testing conditions. Taking into consideration the value division of oxygen index was evaluated according to GB/T 8624-2012:

Grade A incombustible materials: OI > 32%
Grade B1 flame retardant materials: 27% ≤ OI ≤ 32%
Grade B2 flammable materials: 23% ≤ OI ≤ 26%
Grade B3 highly flammable materials: OI ≤ 22%.

In the OI test, the CNF aerogel remained in the group of easily and highly flammable materials (OI = 18.9%) and the composite aerogel CS50-T2.5 remained in the group of flammable materials (OI = 25.2%); the burning level of CS50-T2.5 has rose to a higher grade than that of CNF aerogel. The comparison of the oxygen index of samples CNF and CS50-T2.5 indicates that the introduction of the silica has improved the fire performance of CNF aerogel. The photographs in Fig. 5 show the result of the combustion process of the CNF aerogel and the composite aerogel CS50-T2.5 when burning on the candle for 2 min. The pure CNF aerogel almost burnt out after 2-min burning, whereas the composite aerogel CS50-T2.5 could retain its shape. And the upper surface of the composite aerogel was left relatively uninfluenced. The intact shape of the composite aerogel was due to the presence of the remaining uniform silica particles within the cellulose network. The fireproof performance of the CNF–silica composite aerogels is remarkable, which solves the cellulose aerogel's inflammability and makes them as the super-insulating and fireproofing materials.

Mechanical properties and contact angle

Figure 6 shows a plot of the compiled data for the compressive properties for the CNF aerogel and CNF–silica composite aerogels. The compressive modulus and strength presented similar tendencies with varied silica content. The presence of silica particles within the cellulose network structure caused a deterioration of the mechanical properties. This behavior is directly related to a poor interfacial adhesion between the mesoporous silica and the cellulosic scaffold. However, the CNF–silica composite aerogel CS50-T2.5 showed similar compression properties to those of the pure CNF aerogel; this is further corroboration of the SEM observation that silica particles were dispersed continuously and homogeneously in the cellulosic skeleton and exhibited better interaction between the two phases when prepared at 2.5 mol L^{-1} TEOS concentration. In other

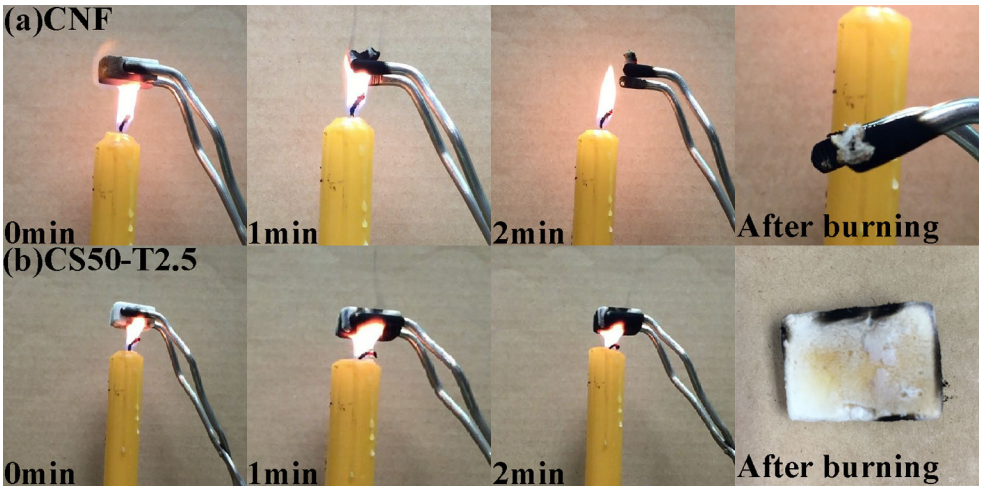

Figure 5 Photographs of the burning process of CNF aerogel and CS50-T2.5 composite aerogel.

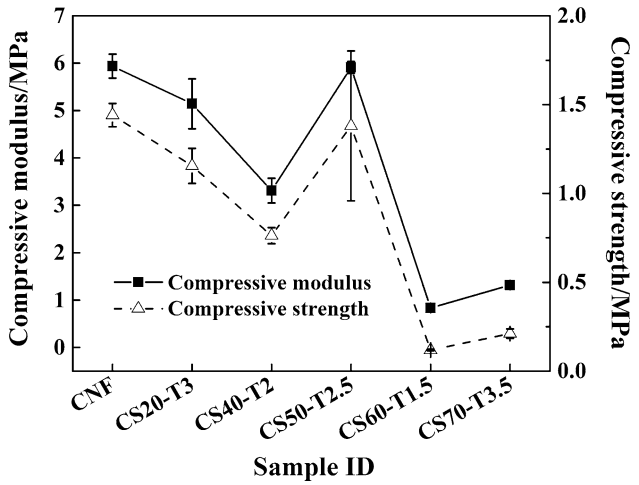

Figure 6 Compressive properties of CNF aerogel and composite aerogels.

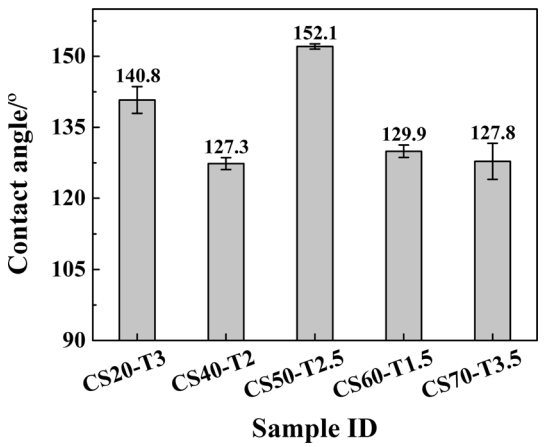

Figure 7 Contact angle of composite aerogels.

concentrations, in the absence of a good nanoscale chemical compatibilization, the cellulose–silica interface was highly discontinuous, hence supporting crack propagation and causing a degradation of the mechanical properties instead of the desired reinforcement. The larger silica content would reveal the brittle and fragile tendency of pure silica aerogel.

The wetting properties of CNF aerogel and CNF–silica composite aerogels were further investigated by static contact angle measurement (Fig. 7). When a water droplet was dropped onto the surface of the CNF aerogel, the droplet instantly spread out and was soaked up immediately by the white porous sponge and could not record the data, indicating a very low contact angle and proving the CNF aerogel's super-hydrophilic character. As expected, all composite aerogels displayed drastically reduced water uptake performance due to the silane layer's being attached to the nanocellulosic scaffold and provoking a hydrophobic property. In line with the analysis of the morphological, thermal, and physical–mechanical properties, the CNF–silica composite aerogel labeled "CS50-T2.5" exhibited better hydrophobic characteristics, and the contact angle was measured at 152.1°.

Conclusions

This paper reports on a thermally stable and hydrophobic CNF–silica composite aerogel prepared by simple immersion of CNF aerogel in an in situ two-step sol–gel silica synthesis process. The effects of different TEOS concentrations for the first step of

silica hydrolysis on the properties of the composite aerogel were investigated. FTIR spectra proved a strong interconnected relationship between the silica particles and the cellulosic scaffold at the chemical molecular level. It was found that the silica content of the composite aerogel and the silica dispersion in the matrix played a vital role in improving the properties of the CNF aerogel and those properties were closely linked to TEOS concentration. The bulk density had a positive relationship with the silica content. The specific surface area also increased with increasing the amount of silica, but the heterogeneous dispersion caused silica agglomeration that would cause a slight decrease in BET surface area. The impregnation of the CNF aerogel with the silica solution caused all the composite aerogels to exhibit better thermal stability and super-hydrophobicity in comparison with pure cellulose aerogel. The pyrolysis temperature increased 31.7 °C higher than CNF aerogel, and the contact angle reached 152.1°. The presence of silica particles in the cellulose scaffold caused a deterioration of the mechanical properties, while the composite aerogel CS50-T2.5 displayed a continuous and homogeneous cellulose–silica interface that had similar mechanical properties to those of pure cellulose aerogel. It can be stated that the CNF–silica composite aerogel prepared at 2.5 mol L^{-1} TEOS concentration possesses thermal stability and hydrophobic characteristics with slightly decreased mechanical properties. Our conclusion is that a cellulose aerogel with improved thermal properties and water resistance may open new opportunities for the application in more widespread functional fields.

Acknowledgements

This work was financially supported by the Special Fund for Forest Scientific Research in the Public Welfare Grant (No. 201504603), the 2014 UTIA Innovation Grant, and Tennessee Experimental Station Project (#TEN00510).

References

[1] Zou J, Liu J, Karakoti AS, Kumar A, Joung D, Li Q, Khondaker SI, Seal S, Zhai L (2010) Ultralight multiwalled carbon nanotube aerogel. ACS Nano 4:7293–7302

[2] Hoepfner S, Ratke L, Milow B (2008) Synthesis and characterisation of nanofibrillar cellulose aerogels. Cellulose 15:121–129

[3] Khare VP, Greenberg AR, Kelley SS, Pilath H, Juhn Roh I, Tyber J (2007) Synthesis and characterization of dense and porous cellulose films. J Appl Polym Sci 105:1228–1236

[4] Heath L, Thielemans W (2010) Cellulose nanowhisker aerogels. Green Chem 12:1448–1453

[5] Chin SF, Binti Romainor AN, Pang SC (2014) Fabrication of hydrophobic and magnetic cellulose aerogel with high oil absorption capacity. Mater Lett 115:241–243

[6] He X, Cheng L, Wang Y, Zhao J, Zhang W, Lu C (2014) Aerogels from quaternary ammonium-functionalized cellulose nanofibers for rapid removal of Cr(VI) from water. Carbohydr Polym 111:683–687

[7] Haimer E, Wendland M, Schlufter K, Frankenfeld K, Miethe P, Potthast A, Rosenau T, Liebner F (2010) Loading of bacterial cellulose aerogels with bioactive compounds by antisolvent precipitation with supercritical carbon dioxide. Macromol Symp 294:64–74

[8] Zaborowska M, Bodin A, Bäckdahl H, Popp J, Goldstein A, Gatenholm P (2010) Microporous bacterial cellulose as a potential scaffold for bone regeneration. Acta Biomater 6:2540–2547

[9] Kobayashi Y, Saito T, Isogai A (2014) Aerogels with 3D ordered nanofiber skeletons of liquid-crystalline nanocellulose derivatives as tough and transparent insulators. Angew Chem Int Ed 53:10394–10397

[10] Sehaqui H (2011) Nanofiber networks, aerogels and biocomposites based on nanofibrillated cellulose from wood. Ph.D. dissertation, KTH School of Chemical Science and Engineering

[11] Yang C, Chen C, Pan Y, Li S, Wang F, Li J, Li N, Li X, Zhang Y, Li D (2015) Flexible highly specific capacitance aerogel electrodes based on cellulose nanofibers, carbon nanotubes and polyaniline. Electrochim Acta 182:264–271

[12] Nemoto J, Saito T, Isogai A (2015) Simple freeze-drying procedure for producing nanocellulose aerogel-containing, high-performance air filters. ACS Appl Mater Int 7:19809–19815

[13] Wang M, Anoshkin IV, Nasibulin AG, Rha R, Nonappa Laine J, Kauppinen EI, Ikkala O (2016) Electrical behaviour of native cellulose nanofibril/carbon nanotube hybrid aerogels under cyclic compression. RSC Adv 6:89051–89056

[14] Wan C, Li J (2015) Embedding ZnO nanorods into porous cellulose aerogels via a facile one-step low-temperature hydrothermal method. Mater Des 83:620–625

[15] Ostrikov K (2005) Reactive plasmas as a versatile nanofabrication tool. Rev Mod Phys 77:489–511

[16] Cervin NT, Aulin C, Larsson PT, Wågberg L (2012) Ultra porous nanocellulose aerogels as separation medium for mixtures of oil/water liquids. Cellulose 19:401–410

[17] Korhonen JT, Hiekkataipale P, Malm J, Karppinen M, Ikkala O, Ras RHA (2011) Inorganic hollow nanotube aerogels by atomic layer deposition onto native nanocellulose templates. ACS Nano 5:1967–1974

[18] Russler A, Wieland M, Bacher M, Henniges U, Miethe P, Liebner F, Potthast A, Rosenau T (2012) AKD-modification of bacterial cellulose aerogels in supercritical CO_2. Cellulose 19:1337–1349

[19] Liu S, Yan Q, Tao D, Yu T, Liu X (2012) Highly flexible magnetic composite aerogels prepared by using cellulose nanofibril networks as templates. Carbohydr Polym 89:551–557

[20] Xia YD, Mokaya R (2004) Ordered mesoporous carbon hollow spheres nanocast using mesoporous silica via chemical vapor deposition. Adv Mater 16:886–891

[21] Cai J, Liu S, Feng J, Kimura S, Wada M, Kuga S, Zhang L (2012) Cellulose–silica nanocomposite aerogels by in-situ formation of silica in cellulose gel. Angew Chem Int Ed 51:2076–2079

[22] Meng Y, Wu Q, Young TM, Huang B, Wang S, Li Y (2017) Analyzing three-dimensional structure and geometrical shape of individual cellulose nanocrystal from switchgrass. Polym Compos 38:2368–2377. https://doi.org/10.1002/pc.23819

[23] Meng Y, Young TM, Liu P, Contescu CI, Huang B, Wang S (2015) Ultralight carbon aerogel from nanocellulose as a highly selective oil absorption material. Cellulose 22:435–447

[24] Fu J, Wang S, He C, Lu Z, Huang J, Chen Z (2016) Facilitated fabrication of high strength silica aerogels using cellulose nanofibrils as scaffold. Carbohydr Polym 147:89–96

[25] Hüsing N, Schubert U, Mezei R, Fratzl P, Riegel B, Kiefer W, Kohler D, Mader W (1999) Formation and structure of gel networks from $Si(OEt)_4/(MeO)_3Si(CH_2)_3NR'_2$ mixtures ($NR'_2 = NH_2$ or $NHCH_2CH_2NH_2$). Chem Mater 11:451–457

[26] Gibson LJ, Ashby MF (1997) Cellular solids: structure and properties. Cambridge University Press, Cambridge

[27] Fu J, He C, Huang J, Chen Z, Wang S (2016) Cellulose nanofibril reinforced silica aerogels: optimization of the preparation process evaluated by a response surface methodology. RSC Adv 6:100326–100333

[28] Ashori A, Sheykhnazari S, Tabarsa T, Shakeri A, Golalipour M (2012) Bacterial cellulose/silica nanocomposites: preparation and characterization. Carbohydr Polym 90:413–418

[29] Lu T, Jiang M, Jiang Z, Hui D, Wang Z, Zhou Z (2013) Effect of surface modification of bamboo cellulose fibers on mechanical properties of cellulose/epoxy composites. Compos B Eng 51:28–34

[30] Shi J, Lu L, Guo W, Zhang J, Cao Y (2013) Heat insulation performance, mechanics and hydrophobic modification of cellulose–SiO_2 composite aerogels. Carbohydr Polym 98:282–289

[31] Zhang W, Zhang Y, Lu C, Deng Y (2012) Aerogels from crosslinked cellulose nano/micro-fibrils and their fast shape recovery property in water. J Mater Chem 22:11642–11650

[32] Sinha E, Rout SK (2008) Influence of fibre-surface treatment on structural, thermal and mechanical properties of jute. J Mater Sci 43:2590–2601. https://doi.org/10.1007/s10853-008-2478-4

[33] Guzun AS, Stroescu M, Jinga SI, Voicu G, Grumezescu AM, Holban AM (2014) Plackett–Burman experimental design for bacterial cellulose–silica composites synthesis. Mater Sci Eng C 42:280–288

[34] Wei T, Chang T, Lu S, Chang Y (2007) Preparation of monolithic silica aerogel of low thermal conductivity by ambient pressure drying. J Am Ceram Soc 90:2003–2007

[35] Liu S, Yu T, Hu N, Liu R, Liu X (2013) High strength cellulose aerogels prepared by spatially confined synthesis of silica in bioscaffolds. Colloids Surf A 439:159–166

[36] He P, Gao X, Li X, Jiang Z, Yang Z, Wang C, Gu Z (2014) Highly transparent silica aerogel thick films with hierarchical porosity from water glass via ambient pressure drying. Mater Chem Phys 147:65–74

[37] He F, Chao S, Gao Y, He X, Li M (2014) Fabrication of hydrophobic silica–cellulose aerogels by using dimethyl sulfoxide (DMSO) as solvent. Mater Lett 137:167–169

[38] Javadi A, Zheng Q, Payen F, Javadi A, Altin Y, Cai Z, Sabo R, Gong S (2013) Polyvinyl alcohol-cellulose nanofibrils-graphene oxide hybrid organic aerogels. ACS Appl Mater Interfaces 5:5969–5975

[39] Okita Y, Saito T, Isogai A (2010) Entire surface oxidation of various cellulose microfibrils by TEMPO-mediated oxidation. Biomacromolecules 11:1696–1700

[40] Tonoli GHD, Teixeira EM, Corrêa AC, Marconcini JM, Caixeta LA, Pereira-da-Silva MA, Mattoso LHC (2012) Cellulose micro/nanofibres from Eucalyptus kraft pulp: preparation and properties. Carbohydr Polym 89:80–88

[41] Wan C, Lu Y, Jiao Y, Cao J, Sun Q, Li J (2015) Preparation of mechanically strong and lightweight cellulose aerogels from cellulose-NaOH/PEG solution. J Sol–Gel Sci Techn 74:256–259